Neutron Scattering Investigation of the Spin Ice State in Dy₂Ti₂O₇.

T. Fennell

The Royal Institution of Great Britain, 21 Albemarle Street, London, W1S 4BS, United Kingdom

O. A. Petrenko* and B. Fåk[†]
ISIS Facility, Rutherford-Appleton Laboratory, Chilton, Didcot, OX11 0QX, United Kingdom

S. T. Bramwell[‡]

Department of Chemistry, University College London, 20 Gordon Street, London, WC1H 0AJ, United Kingdom

M. Enjalran, § T. Yavors'kii, M. J. P. Gingras, ¶ and R. G. Melko**

Department of Physics, University of Waterloo, Ontario, N2L 3G1, Canada

G. Balakrishnan

Department of Physics, University of Warwick, Coventry, CV4 7AL, United Kingdom (Dated: February 8, 2020)

 $\mathrm{Dy_2Ti_2O_7}$ has been advanced as an ideal spin ice. We present a neutron scattering investigation of a sample of $^{162}\mathrm{Dy_2Ti_2O_7}$. The scattering intensity has been mapped in zero applied field in the hhl and hk0 planes at temperatures between 0.05 K and 20 K. The measured diffuse scattering (in the static approximation) has been compared to that predicted by the dipolar spin ice model. The comparison is good, except at the Brillouin zone boundaries where extra scattering appears in the experimental data. It is concluded that the dipolar spin ice model provides a successful basis for understanding $\mathrm{Dy_2Ti_2O_7}$, but that there are issues which remain to be clarified.

PACS numbers: 75.50Lk, 75.40Cx, 75.25+z

I. INTRODUCTION

The concept of spin ice¹ has appeared recently as a result of a direct analogy between the statistical mechanics of O-H bonds in Pauling's model of water $ice^{2,3}$ and those of the localized magnetic moments of some highly frustrated magnets^{1,4,5}. These materials, typified by Ho₂Ti₂O₇¹, Dy₂Ti₂O₇⁴ and Ho₂Sn₂O₇⁶, provide almost ideal experimental realizations of spin ice, a magnetic "sixteen vertex" model⁷. Their temperature-field phase diagrams are exceedingly rich and have revealed several new magnetic phases and transitions^{1,8,9,10,11}. The magnetic dynamics of the spin ices also show some unique properties including a crossover from Debye-like spin relaxation^{12,13,14} to quantum tunnelling dynamics ^{15,16} at the unusually high temperature of 15 K. The current paper builds on earlier work^{1,6,17,18} to characterize the neutron scattering of spin ice materials. In it, we report the first neutron scattering images of the spin ice state of Dy₂Ti₂O₇ ¹⁹ which are compared with theoretical pre $dictions^{20,21,22}$

In $\mathrm{Dy_2Ti_2O_7}$, as well as in the other spin ice materials $\mathrm{Ho_2Ti_2O_7}$ and $\mathrm{Ho_2Sn_2O_7}$, the rare earth moments ('spins') are arranged on a pyrochlore lattice of linked tetrahedra (see figure 1). Strong crystal field anisotropy²³ confines each spin as an Ising-like doublet to the local trigonal $\langle hhh \rangle$ axis that connects the center of the elementary tetrahedron to its vertex. With this constraint and ferromagnetic coupling, the magnetic ground state of a single tetrahedron is defined by a "two spins"

FIG. 1: The pyrochlore lattice (top) and the spin ice state on a single tetrahedron (bottom). A macroscopic spin ice state is constructed by stacking such local arrangements on the lattice.

in, two spins out" rule, analogous to the Bernal-Fowler ice rule that controls the proton arrangements in water ice^{24} . This rule minimizes (within the constraints of the anisotropy) only four of the six near neighbor magnetic interactions and so the system is highly frustrated, sharing with ice the property of zero point entropy^{1,2,3,4}. In the spin ice materials, the ferromagnetic near neighbor coupling arises from the strong dipole-dipole interaction between neighboring spins²⁰. If the dipolar interaction is truncated at nearest neighbors one has the "near neighbor" spin ice model^{1,7} (note that dipole interactions are equivalent to exchange terms for Ising systems). This approximation captures the bulk properties of the spin ice materials^{1,4,25,26,27} and gives a qualitative description of the microscopic spin correlations, as determined by neutron scattering 1,17 .

The subject of this paper, $\mathrm{Dy_2Ti_2O_7}$, has previously been investigated by bulk methods 4,12,27,28 . In zero field, the specific heat resembles a Schottky anomaly, peaking at 1.24 K and falling to zero at lower temperatures. Unlike its holmium analogue, which shows an extra peak due to freezing of the nuclear spins 17,29 , $\mathrm{Dy_2Ti_2O_7}$ shows no other specific heat contributions down to 0.2K, where

Isotope	Natural	Sample	σ_a
	Abundance	Content	(barn)
	(%)	(%)	
Natural		_	994.(13.)
¹⁵⁶ Dy	0.06	< 0.01	33.(3.)
¹⁵⁸ Dy	0.1	< 0.01	43.(6.)
¹⁶⁰ Dy	2.34	0.02	56.(5.)
¹⁶¹ Dy	19	0.47	600.(25.)
¹⁶² Dy	25.5	96.8	194.(10.)
¹⁶³ Dy	24.9	2.21	124.(7.)
¹⁶⁴ Dy	28.1	0.5	2840.(40.)
Sample		_	207.6

TABLE I: Isotopic abundances and absorption cross sections (σ_a) of natural dysprosium and the enriched sample used in these experiments³¹.

the specific heat becomes exponentially small. It has thus proved highly favorable for bulk measurements, having been used to estimate the zero point entropy in zero field⁴, and to demonstrate the existence of "kagome ice", a field induced state that retains zero point entropy^{9,28}. However, owing to its large neutron absorption, $\mathrm{Dy_2Ti_2O_7}$ has not yet been extensively studied by neutron scattering¹⁹, the technique that was crucial in establishing the existence of the spin ice state in $\mathrm{Ho_2Ti_2O_7}^{1,17}$ and $\mathrm{Ho_2Sn_2O_7}^6$.

To address the problem of large neutron absorption in natural dysprosium based materials we have grown an isotopically enriched crystal of Dy₂Ti₂O₇ specifically for use in neutron scattering experiments. The details of the sample and the experiments performed on it, are given in section IIA. The experiments were designed to examine the nature of the presumed spin ice state that is established when the sample is cooled in zero applied magnetic field^{4,20}. The data were modelled using the "dipolar" spin ice model that considers further neighbor dipole-dipole interactions as well as a small antiferromagnetic exchange coupling that can be estimated by fitting the susceptibility³⁰ or specific heat²⁰. Solution of this model presents some complications. It has been established that simple truncation of the dipolar interaction³⁰ leads to ordered states that are not observed experimentally. In contrast, Ewald summation techniques²⁰ give a close agreement with experiment and explain the success of the near neighbor model in terms of self-screening of the long range part of the dipolar interaction. Details of the dipolar spin ice model, as applied to Dy₂Ti₂O₇, are given in section IIB of the current paper, while the comparison of theory and experiment is given in section III. The paper is concluded with a discussion of the results, section IV.

II. EXPERIMENTAL

A. Neutron Scattering

Neutron scattering measurements were carried out on PRISMA at the ISIS pulsed neutron source of the Rutherford-Appleton Laboratory. A pulsed white neutron beam is incident on the sample. PRISMA views a cold (95 K) methane moderator and a supermirror guide system, providing a high flux of long wavelength neutrons, allowing measurement at relatively low $|\mathbf{Q}|$. The neutrons scattered from the sample are recorded in sixteen detectors which cover a range of 16° in scattering angle. From the neutron time of flight, the scattering angle, and the orientation of the sample with respect to the incoming beam, the scattered intensity can be determined as a function of the position in reciprocal space. By rotating the crystal about the vertical axis intensity maps covering a large region of the scattering plane can be constructed. This method is particularly useful for studies of diffuse magnetic scattering. The average scattering angle ϕ of the sixteen detectors used for the measurements is chosen as a compromise between flux (at a given wavevector) and background (due to air scattering). The advantages of measuring the diffuse magnetic neutron scattering on PRISMA have been clearly demonstrated using the example of Ho₂Ti₂O₇, where the dipolar spin ice nature of the zero field spin correlations has been unambiguously established¹⁷. In that and the current experiment the neutron scattering is measured in the static approximation 32 .

Natural dysprosium contains seven isotopes, several of which absorb neutrons quite strongly. This can make the detection of weaker effects like diffuse scattering difficult or impossible. To reduce this, an isotopically enriched sample was used. The natural abundances, scattering lengths and cross sections for natural dysprosium and our sample are given in table I. The absorption cross-section σ_a is reduced by a factor of 4.8 using the ¹⁶²Dy isotope compared to natural Dy. Since absorption attenuates scattered intensity by a factor of the form $\exp(-N\sigma_a\lambda)$ (where N is the number density of scatterers per unit volume, σ_a is the absorption cross section, usually tabulated for 2200 m s⁻¹ neutrons, and λ is the neutron wavelength scaled to the value used in σ_a) this makes a significant difference at long wavelengths.

A large high quality single crystal was grown using an infra-red double mirror image furnace³³. The crystal has a diameter of ≈ 0.4 cm, length ≈ 1.5 cm, and is translucent amber-red in color. It has a cylindrical form typical of image furnace grown crystals. The crystal was varnished into a large copper support to ensure good thermal contact.

Using a $^3\mathrm{He}$ sorption refrigerator insert in an Orange cryostat, the hhl plane was mapped in zero field at 20 K and 0.3 K using the average scattering angle $\phi = -48^\circ$. The same plane was mapped at 0.3 K and 1.3 K using the average scattering angle $\phi = -32^\circ$. Using a dilution

refrigerator insert in an Oxford Instruments cryomagnet the hk0 and hhl planes were mapped in zero field at 0.05 K. These maps are shown in figure 2. All parts of the sample environment in the beam were made of aluminium (other than the copper support), which gives rise to powder lines at $|\mathbf{Q}| = 2.70$, 3.12 and 4.40 Å⁻¹.

Standard data reduction procedures were applied to transform time of flight and angle information to reciprocal space, to correct for absorbtion in the sample, and to normalize the data to an absorption corrected vanadium run. The latter corrects for the wavelength-dependent flux profile and detector efficiency. Despite the five-fold reduction in absorption compared to natural dysprosium, the data analysis procedure revealed that absorption by the Dy₂Ti₂O₇ crystal was still significant and needed to be taken into account. The absorption correction was made by calculating an attenuation coefficient $(A(s,\phi))$ by which the data could be divided. The coefficient for a cylinder of radius R was originally derived by Sears³⁴ and is

$$A(s,\phi) = [1 + 4bs^2 - 0.5s^2\cos^2(\phi/2)] \times \exp(-2as), (1)$$

where $a = 8/3\pi$, $b = (1 - a^2)/2$, $s = \mu R$ and ϕ is the scattering angle. In this formula, μ , the absorption coefficient, depends on both the scattering cross section, and the wavelength dependent absorption cross section.

B. Monte Carlo Simulations

To model our experimental data for $Dy_2Ti_2O_7$, we use a Hamiltonian appropriate for the $\langle 111 \rangle$ Ising pyrochlores:

$$H = -J \sum_{\langle (i,a),(j,b)\rangle} \mathbf{S}_i^a \cdot \mathbf{S}_j^b \tag{2}$$

$$+DR_{\text{nn}}^{3} \sum_{(i,a)>(j,b)} \left(\frac{S_{i}^{a} \cdot S_{j}^{b}}{|R_{ij}^{ab}|^{3}} - \frac{3(S_{i}^{a} \cdot R_{ij}^{ab})(S_{j}^{b} \cdot R_{ij}^{ab})}{|R_{ij}^{ab}|^{5}} \right),$$

where $S_i^a = \hat{z}^a \sigma_i^a$ represents an Ising moment of magnitude $|S_i^a| = 1$ at fcc lattice site i and tetrahedral basis position a, with its quantization axis (\hat{z}^a) oriented along the local (111) direction, and $\sigma_i^a = \pm 1$. The nearest neighbor exchange energy is $J_{\rm nn} = J/3$, and the nearest dipole-dipole strength is $D_{\rm nn} = 5D/3$, where $D = (\mu_o/4\pi)\mu^2/R_{\rm nn}^3$ and μ is the moment of the Dy³⁺ ion. The vector separation between moments S_i^a and S_j^b is R_{ij}^{ab} .

We simulate Eq. 2 on a pyrochlore lattice of $4\times4\times4$ cubic cells (N=1024 spins) with periodic boundary conditions. The long-range nature of the dipole-dipole interactions are properly handled by using standard Ewald techniques for real space dipoles²⁰. Our model employs energy parameters appropriate for Dy₂Ti₂O₇, $J_{\rm nn}=-1.24{\rm K}$ and $D_{\rm nn}=2.35{\rm K}^{20}$.

At the temperatures of interest the system is only able to access states within the spin ice manifold. Single spin flip dynamics require the introduction of ice rule defects. This means that the acceptance rate of single spin flips becomes extremely small and ability to equilibrate the system below 0.3 K becomes dubious. In order to improve on approach to equilibrium of this paramagnetic regime of the dipolar spin ice, dynamics was restored by using a loop algorithm²¹. To produce scattering data the system was placed in the ordered groundstate found by Melko et al. 21 , at 0.4 K. 5×10^6 Monte Carlo steps (MCS) per spin and 5×10^6 loop attempts were made to equilibrate the system and bring it to a paramagnetic state. Loop attempts were therefore separated by N = 1024MCS. The system was then cooled to 0.3 K where the same number of single spin flip and loop attempt steps were used for equilibration and then data collection at 0.3 K. See Refs. 17,20,35 for more details. This procedure guarantees that the maximum level of spin-spin correlation can develop in the Monte Carlo simulation. The motivation for this procedure is further discussed in $Ref.^{36}$.

There are 12 symmetry related ordered stuctures and each was used as a start point for a simulation. We calculate the neutron scattering intensity, $I(\mathbf{Q})$, at $T=0.3\mathrm{K}$ from 200 independent spin configurations derived from each starting structure using the formula

$$I(\mathbf{Q}) \propto \frac{|f(Q)|^2}{N} \sum_{(i,a),(j,b)} e^{i\mathbf{Q}\cdot\mathbf{R}_{ij}^{ab}} \langle \mathbf{S}_{i,\perp}^a \cdot \mathbf{S}_{j,\perp}^b \rangle ,$$
 (3)

where $\langle ... \rangle$ denotes a thermal average, $S_{i,\perp}^a$ is the spin component perpendicular to the scattering wave vector \mathbf{Q} , and f(Q) is the magnetic form factor for Dy^{3+17} . The Monte Carlo results for $I(\mathbf{Q})$ are compared to the experimental data in the (hhl) and (hk0) planes below. The simulations are nominally at 0.3 K, whereas the experimental data was collected at either 0.3 K (hhl) plane) or 0.05 K (hk0) plane). We consider it valid to make these comparisons because below 0.4 K the susceptibility²⁷ and neutron scattering intensity, $I(\mathbf{Q})$, and specific heat⁴ do not change significantly and the system essentially appears to be frozen with negligible thermal spin fluctuations.

III. RESULTS

In this section, the observed magnetic diffuse scattering is presented and compared to Monte Carlo simulations where possible. The temperature dependence of the scattering in the hhl plane is discussed first (section III A), in order to establish the temperature regimes of interest. In the following sections (III B and III C) the scattering intensity measured at base temperature is compared to Monte Carlo simulations. Finally, section III D is concerned with features in the experimental scattering which are not reproduced by the model.

A. Temperature Dependence of the Diffuse Scattering

The temperature dependence of the diffuse scattering due to the development of ice rule fulfilling spin correlations was sampled at four temperatures for the hhl plane (20, 1.3, 0.3 and 0.05 K, see figure 2). An important point that can be obtained from these measurements is that the diffuse scattering does evolve with temperature. As the sample is cooled, no diffuse scattering characteristic of spin ice correlations has built up by 20 K. This is entirely expected as the bulk susceptibility shows that Dv₂Ti₂O₇ is paramagnetic at this temperature²⁷. At 1.3 K strong diffuse scattering has appeared. The form is closely similar to that of the near-neighbor spin ice as simulated in Ref¹⁷. Between 1.3 and 0.3 K the spin correlations evolve and additional features appear in the scattering pattern, as discussed below. The scattering at 0.05 K throughout the hhl plane (not illustrated here) is not significantly different to that at 0.3 K.

B. Scattering in the hk0 plane

For the hk0 plane data has only been collected at 0.05 K. For the hk0 plane the simulation and the experiment seem to agree very well indeed. The two scattering maps are shown in figure 3. A comparison by a cut through the data is shown in fig 4. The Monte Carlo pattern has been fitted to the experimental diffuse scattering using a flat background and a scaling parameter.

C. Scattering in the hhl plane

For the hhl plane direct comparison of the experimental and simulated scattering maps reveals both close similarities and significant differences. The two scattering patterns are shown in figure 2. It is apparent that whilst the experimental pattern does contain the features of the dipolar spin ice scattering (for example the large diffuse feature at 003) it also contains features that are are not reproduced by the simulation. These extra features are concentrated around the boundaries of the Brillouin zones

The similarities and differences of the observed and calculated patterns are more clearly emphasized in figure 4. Here slices through the data have been made. The agreement along the [hh0] and [00l] is good. The slice along [hh2.3] is chosen to highlight the differences and it can be seen that where the slice crosses the zone boundary the form of the calculated and experimental intensities is significantly different.

D. Zone Boundary Features

One possible explanation for the zone boundary features is that they are due to phonons. However, the following facts suggest that the intensity is magnetic: (1) the scattering appears as temperature is decreased; the converse would be expected for a phonon; (2) the experimentally observed features fall off with increasing $|\mathbf{Q}|$, which is not expected for phonons.

The second point can be demonstrated by comparison of the intensity of the feature with the magnetic form factor of Dy^{3+} . If the intensity at equivalent points on successive zone boundaries is compared it would be expected to follow the form factor if the scattering process is magnetic. On the basis of this comparison it seems entirely reasonable to attribute the zone boundary features to a magnetic correlation.

IV. DISCUSSION

The dipolar spin ice model apparently provides a very successful model for the zero field spin correlations in Dy₂Ti₂O₇. However, some additional spin correlations do occur which are not captured by the model. The model is very successful in describing the bulk and microscopic data for Ho₂Ti₂O₇¹⁷, and the bulk data for Dy₂Ti₂O₇²⁰. One might therefore ask, how this further restriction of the dipolar spin ice manifold is not manifested in the fit to the heat capacity?

In answer to this question, it should be noted that the fit to the heat capacity 20 is not perfect: the experiment and simulation differ in detail. The fact that the zone boundary features are very diffuse in reciprocal space and run all around the zone boundaries, suggests that the associated spin correlations are short ranged and symmetric. A small difference between the experimental and theoretical heat capacities is therefore understandable since the extra spin correlations need not make a major contribution to the entropy. We therefore conclude that the neutron scattering and specific heat data 4,20 are consistent.

A clue to the origin of the extra spin correlations is the fact that they are much less evident in Ho₂Ti₂O₇ ^{17,18}, even if they cannot be excluded completely within experimental error. According to the model, the principal difference between Ho₂Ti₂O₇ and Dy₂Ti₂O₇ is the much more significant antiferromagnetic exchange term in the spin Hamiltonian of Dy₂Ti₂O₇. Several possibilities arise. Firstly, this exchange term was simply invoked to fit bulk measurements^{20,27,30}, which are not sensitive to the details of a Hamiltonian in the way that diffuse neutron scattering is. Hence the extra scattering might reveal that extra, or different terms are required in the model Hamiltonian: for example, it might be necessary to include further neighbor exchange interactions. Further theoretical work is required to distinguish various possibilities.

FIG. 2: Dy₂Ti₂O₇: Diffuse scattering in the hhl plane measured at 20 K (top left), 1.3 K (top right) and 0.3 K (bottom left). The sharp, intense spots are nuclear Bragg reflections with no magnetic intensity. The map at 20 K was recorded using an average scattering angle of $\phi = 48^{\circ}$ which shifts the scattering to larger values of hhl compared to $\phi = 32^{\circ}$. Therefore this map contains a region of arc shaped artefacts and zero intensity where the neutron flux tailed off. The result of the Monte Carlo simulation of the dipolar spin ice model at 0.3 K is shown at bottom right.

FIG. 3: Dv₂Ti₂O₇ at0.05experimental scattering intensity inthe hk0plane (left). compared with that calculated from Monte Carlo simulations (right).

Zone boundary scattering has recently also been observed in the hk0 plane for $\rm ZnCr_2O_4$ ³⁷ and the hhl plane for $\rm ZnFe_2O_4$ ³⁸. We suggest that while the three magnets are quite different the zone boundary features may also be a generic feature of frustrated magnets due to the formation of local spin clusters such as the "quantum protectorate" in $\rm ZnCr_2O_4$ ³⁷.

One might also consider the possibility that the difference between the experimental and calculated scattering is due to lack of thermal equilibrium in the experimental system. The spin dynamics evidently become very slow below $T\approx 0.5$ K, so it is possible that the sample is thermally quenched into a defective spin ice state. Defects might include local breaking of the ice rules, which cannot be relaxed, due to the frozen dynamics. These could cause the departure of the data from the experimental pattern.

In conclusion, we have presented a systematic investigation of the diffuse scattering of $\mathrm{Dy_2Ti_2O_7}$ in zero magnetic field. We have observed three regimes of behavior. At 20 K the spins are paramagnetic, without spin ice correlations, which should help interpret recent bulk susceptibility measurements of the dynamical properties 12,13,27 , which have been discussed in terms of both correlated and uncorrelated dynamical processes 13,15,16 .

At 1.3 K the spin correlations are similar to those of the near neighbor spin ice model, suggesting that further neighbor dipole interactions are not strongly relevant in this temperature range. At 0.3 K the scattering is modified to correspond quite closely to the frozen state of the dipolar spin ice model, with effective infinite range interactions. However, in this temperature range we have observed additional scattering features around the zone boundary which for the time being remain unexplained. Further calculations are in progress to clarify their origin.

V. ACKNOWLEDGEMENTS

We thank the sample environment team at ISIS, in particular Richard Down and Dave Bates, and Martyn Bull for assistance on PRISMA. TF acknowledges the EPSRC for funding, and Andrew Harrison for hospitality in Edinburgh whilst this work was written up. Work done at the University of Warwick was funded by an EPSRC grant. Work done at the University of Waterloo has been supported by the NSERC of Canada, the Canada Research Chair Program, the Province of Ontario, and Research Corporation.

^{*} Now at Department of Physics, University of Warwick, Coventry, CV4 7AL, United Kingdom

[†] Now at CEA Grenoble, DRFMC/SPSMS, 38054, Grenoble, Cedex 9, France

[‡] Electronic address: s.t.bramwell@ucl.ac.uk

[§] Now at Department of Physics, Southern Connecticut State University, New Haven, CT 06515, USA

[¶] Also at Canadian Institute for Advanced Research, 180 Dundas Street West, Toronto, Ontario, M5G 1Z8, Canada

^{**} Now at Department of Physics, University of California, Santa Barbara, CA 93106-9350, USA

¹ M. J. Harris, S. T. Bramwell, D. F. McMorrow, T. Zeiske, and K. W. Godfrey, Phys. Rev. Lett. **79**, 2554 (1997).

² L. Pauling, J. Am. Chem. Soc. **57**, 2680 (1935).

³ W. F. Giauque and J. W. Stout, J. A., Chem. Soc. 58, 1144 (1936).

⁴ A. P. Ramirez, A. Hayashi, R. J. Cava, R. Siddharthan, and B. S. Shastry, Nature **399**, 333 (1999).

⁵ S. T. Bramwell and M. J. P. Gingras, Science **294**, 1495 (2001).

⁶ H. Kadowaki, Y. Ishii, K. Matsuhira, and Y. Hinatsu, Phys. Rev. B **65**, 144421 (2002).

⁷ S. T. Bramwell and M. J. Harris, J. Phys.: Condens. Mat. 10, L215 (1998).

⁸ M. J. Harris, S. T. Bramwell, P. C. W. Holdsworth, and J. D. M. Champion, Phys. Rev. Lett. 81, 4496 (1998).

⁹ K. Matsuhira, Z. Hiroi, T. Tayama, S. Takagi, and T. Sakakibara, J. Phys.: Condens. Mat. 14, L559 (2002).

¹⁰ T. Sakakibara, T. Tayama, Z. Hiroi, K. Matsuhira, and S. Takagi, Phys. Rev. Lett. **90**, 207205 (2003).

¹¹ R. Moessner and S. L. Sondhi, arXiv:cond-mat/p. 0303210 (2003).

¹² K. Matsuhira, Y. Hinatsu, and T. Sakakibara, J. Phys.: Condens. Mat. 13, L737 (2001).

¹³ J. Snyder, J. S. Slusky, R. J. Cava, and P. Schiffer, Nature 413, 48 (2001).

¹⁴ J. Snyder, J. S. Slusky, R. J. Cava, and P. Schiffer, Phys. Rev. B **66**, 064432 (2002).

¹⁵ G. Ehlers, A. L. Cornelius, M. Orendáč, M. Kajčnacová, T. Fennell, S. T. Bramwell, and J. S. Gardner, J. Phys.:

FIG. 4: $Dy_2Ti_2O_7$ at 0.3 K: comparison of experimental and Monte Carlo data for hk0 and hhl planes. The comparison in the hk0 plane is shown at top left using a slice along [3k0]. The Monte Carlo data was compared to the experimental data by adjusting a scaling factor and single background parameter in order to give the best fit. The comparisons for the hhl plane are slices along [hh0] (top right), [00l] (bottom left) and along [hh2.3] (bottom right). For slices 2 and 3 the Monte Carlo data were compared using a scale factor and sloping background, slice 4 was compared with a scale factor and constant background. The slice positions in the scattering plane are indicated in the insets, and for the hhl plane by numbers 2-4. Shaded areas in the slices are Bragg peaks from the sample and were excluded from the fitting.

Condens. Mat. 15, L9 (2003).

¹⁶ J. Snyder, B. G. Ueland, J. S. Slusky, H. Karunadasa, R. J. Cava, A. Mizel, and P. Schiffer, Phys. Rev. Lett. 91, 107201 (2003).

¹⁷ S. T. Bramwell, M. J. Harris, B. C. den Hertog, M. J. P. Gingras, J. S. Gardner, D. F. McMorrow, A. R. Wildes, A. L. Cornelius, J. D. M. Champion, R. G. Melko, et al., Phys. Rev. Lett. 87, 047205 (2001).

¹⁸ M. Kanada, Y. Yasui, Y. Kondo, S. Iikubo, H. Harashina, M. Sato, H. Okumura, K. Kakurai, and H. Kadowaki, J. Phys. Soc. Jpn. **71**, 313 (2002).

A. preliminary communication of this work appeared in: T. Fennell, O. A. Petrenko, G. Balakrishnan, S. T. Bramwell, J. D. Champion, B. Fåk, M. J. Harris, and D. McK. Paul, Appl. Phys. A 74, S889 (2002).

²⁰ B. C. den Hertog and M. J. P. Gingras, Phys. Rev. Lett. 84, 3430 (2000).

²¹ R. G. Melko, B. C. den Hertog, and M. J. P. Gingras, Phys. Rev. Lett. **87**, 067203 (2001).

²² M. Enjalran and M. J. P. Gingras, arXiv:cond-mat/p. 0307151 (2003).

²³ S. Rosenkranz, A. P. Ramirez, A. Hayashi, R. J. Cava, R. Siddharthan, and B. S. Shastry, J. Appl. Phys. **68**, 855 (1992).

²⁴ J. D. Bernal and R. H. Fowler, J. Chem. Phys. **1**, 515 (1933).

²⁵ A. L. Cornelius and J. S. Gardner, Phys. Rev. B **64**, 060406(R) (2001).

²⁶ O. A. Petrenko, M. Lees, and G. Balakrishnan, Phys. Rev. B 68, 012406 (2003).

²⁷ H. Fukazawa, R. G. Melko, R. Higashinaka, Y. Maeno, and M. J. P. Gingras, Phys. Rev. B **65**, 054410 (2002).

²⁸ R. Higashinaka, H. Fukazawa, and Y. Maeno, Phys. Rev. B **68**, 014415 (2003).

²⁹ B. C. den Hertog, M. J. P. Gingras, S. T. Bramwell, and M. J. Harris, arXiv:cond-mat/p. 9912220 (1999).

³⁰ R. Siddharthan, B. S. Shastry, A. P. Ramirez, A. Hayashi, R. J. Cava, and S. Rosenkranz, Phys. Rev. Lett. 83, 1854 (1999).

³¹ A. Munter, Neutron scattering lengths and cross sections, (www.ncnr.nist.gov).

³² M. F. Collins, Magnetic Critical Scattering (Oxford University Press, Oxford, 1989).

³³ G. Balakrishnan, O. A. Petrenko, M. R. Lees, and D. M. Paul, J. Phys.: Condens. Mat **10**, L723 (1998).

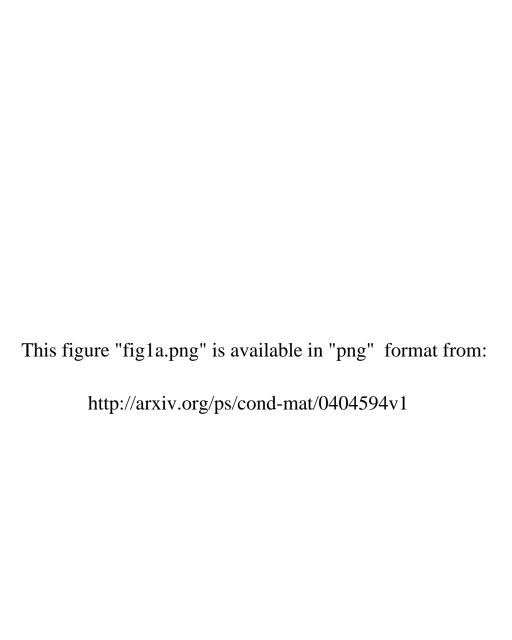
³⁴ V. F. Sears, J. Appl. Cryst. **17**, 226 (1984).

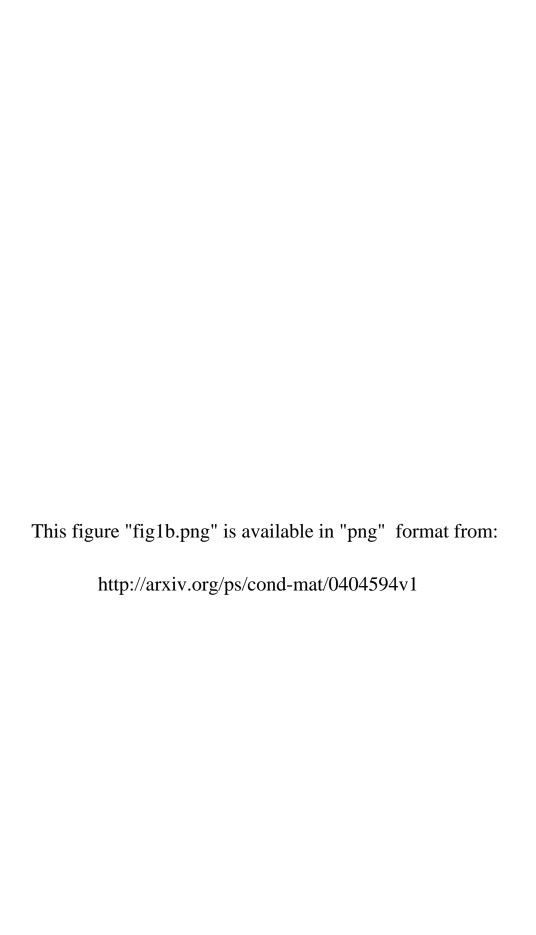
R. Melko, M. Enjalran, B. den Hertog, and M. Gingras, arXiv:cond-mat/p. 0308282 (2003).

³⁶ It is now rather well established that the dipolar spin ice model possesses long-range order at sufficiently low temperatures which is established via a sharp and strongly first order phase transition²¹. The critical temperature for this

transition is independent of exchange coupling J, and is set only by the dipole coupling D, with $T_c/J \sim 0.13 \sim 180 \text{ mK}$ for both Dv₂Ti₂O₇ and Ho₂Ti₂O₇. This transition occurs in the model provided thermal equilibrium can be maintained at low temperatures, well below the temperature, T_b at which the barriers that originate from the creation of the ice-rule manifold rapidly develop. One can associate this barrier-formation temperature, T_b , to the peak of the experimental specific heat, T_{peak} . For $\text{Dy}_2\text{Ti}_2\text{O}_7$, $T_{\rm peak} \sim 1.24$ K while $T_{\rm peak} \sim 1.9$ K for Ho₂Ti₂O₇. In a previous work ¹⁷, we compared the experimental neutron scattered intensity results for Ho₂Ti₂O₇ with a conventional Monte Carlo simulation using conventional spin flip mechanism and no loop moves. The motivation behind such comparison is that T_c is much lower than T_{peak} for $\text{Ho}_2\text{Ti}_2\text{O}_7$. As such, the spin dynamics freezes out in Ho₂Ti₂O₇ at sufficiently high temperature compared to T_c that extended short range order has not yet developed, especially given that the transition is first order. For $Dy_2Ti_2O_7$, T_{peak} is lower, and one expects that the material can maintain equilibrium to somewhat lower temperature than Ho₂Ti₂O₇, and possibly develop "better" correlations upon approaching the putative $T_c \sim 180$ mK. We therefore make the assumption that experimentally, Dy₂Ti₂O₇ is still maintaining a reasonable level of thermal equilibrium at the temperature T=0.3 for which we are comparing experimental I(Q) with Monte Carlo simulations. On the other hand, one cannot maintain equilibrium effectively for simulations of Dy₂Ti₂O₇ down to 0.3 K using the single spin flip Metropolis algorithm. Consequently, to bring the simulation of Dv₂Ti₂O₇ at 0.3 K to a level of equilibration on par with that which we are ascribing to the real material, we use the loop simulations. Clearly, such reasoning must break down as the temperature at which we want to compare experiment with simulation is decreased toward T_c , since the real material does not develop the long-range order predicted to develop at 180 mK down to 50 mK (possibly because it falls out of equilibrium between 180 mK and 300 mK), while the loop Monte Carlo would develop such order. As discussed in the main text, it appears that the experiment develops more correlations than the simulations do, and not the converse, as would have been the case had we innappropriately biased the simulation towards a higher level of equilibrium than the one exhibited by the real material due to the usage of loop moves. It is this higher level of correlations found in the experiments compared to the simulations that introduces the problem and puzzle exposed in this paper and addressed in the discussion section.

³⁷ S.-H.Lee, C. L. Broholm, W. Ratcliff, G. Gasparovic, Q. Huang, T. H. Kim, and S.-W. Cheong, Nature 418, 856 (2002). 38 K. Kamazawa, Y. Tsunoda, H. Kadowaki, and K. Kohn, Phys. Rev. B ${\bf 68},\,024412$ (2003).





This figure "fig2a.png" is available in "png" format from:

This figure "fig2b.png" is available in "png" format from:

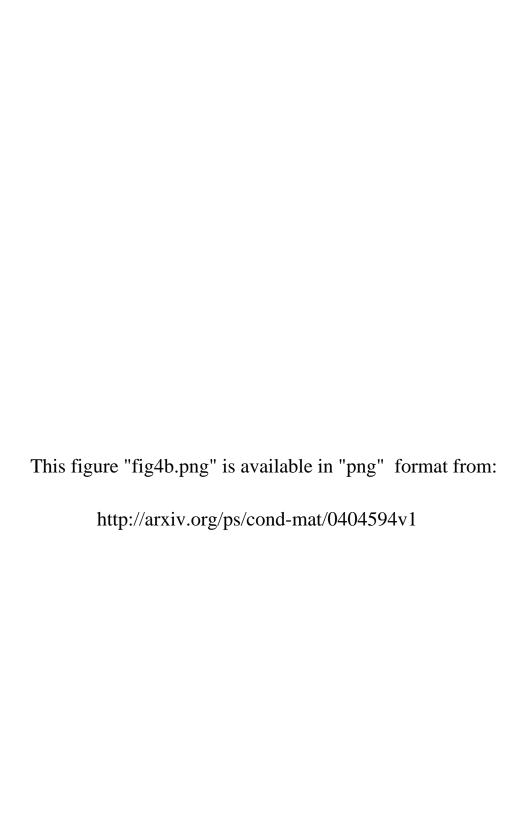
This figure "fig2c.png" is available in "png" format from:

This figure "fig2d.png" is available in "png" format from:

This figure "fig3a.png" is available in "png" format from:

This figure "fig3b.png" is available in "png" format from:

This figure "fig4a.png" is available in "png" format from: http://arxiv.org/ps/cond-mat/0404594v1



This figure "fig4c.png" is available in "png" format from:

